

Direct space to time terahertz pulse shaping with nonlinear metasurfaces

SHAY KEREN-ZUR^{1,2,*} AND TAL ELLENBOGEN^{1,2}

¹*Department of Physical Electronics, School of Electrical Engineering, Tel-Aviv University, Tel Aviv, 6997801, Israel*

²*Center for Light-Matter Interaction, Tel-Aviv University, Tel-Aviv 6779801, Israel*

**shaykerenzur@tauex.tau.ac.il*

Abstract: We present a method for the generation of THz pulses with tailored temporal shape from nonlinear metasurfaces. The method is based on single-cycle THz emission by the metasurface inclusions. We show that the spatial amplitude and phase structure of the nonlinear response is mapped to the temporal shape of pulses emitted at certain angles. We specifically show a method for reconstruction of desired pulses, generation of few-cycles pulses with tailored carrier-envelope and all-optical control over the pulse shape by the pump pulse characteristics.

© 2019 Optical Society of America under the terms of the [OSA Open Access Publishing Agreement](#)

1. Introduction

The capability to form the temporal profile of terahertz waves (0.1-10 THz band) is essential for numerous applications. In THz time domain spectroscopy, pulse shaping shows great advantages, as it allows to obtain coherent control over quantum system. Multidimensional molecular spectroscopy [1–3], magnetic spin waves manipulation [4,5], molecular alignment [6], and control over semiconductor qubits [7] were demonstrated, just to name a few. Finally, pulse shaping techniques in the THz regime can be also useful for development of fast wireless communication links [8,9].

While pulse shaping techniques are well-explored and utilized over the entire optical regime [10–12], in the THz band, where generation, manipulation and detection of radiation is significantly more challenging, pulse-shaping techniques are still limited [13–20]. Partial THz pulse shaping capabilities were demonstrated by using passive and active filters, based on metamaterial or various photonic structures [21–24]. More extended pulse shaping capabilities were demonstrated based on temporal shaping of ultrashort optical pulses, used for the generation of THz waves in photoconductive antennas or nonlinear crystals [13–15]. In addition, engineered poling of ferroelectric crystals was used for the generation of shaped THz pulses [16,25], and also spatially controlled photo-injected charge carriers in waveguides were used for the excitation of arbitrary phase controlled pulse trains [17,18].

Recently it was shown that single- and few-cycles THz pulses with pre-designed spatial profile can be generated by nonlinear metasurfaces (NLMS) [26]. The metasurface is composed of meta-atoms with resonant behavior at the near infrared (NIR), for enhanced nonlinear interaction at the resonance frequency. The metasurface is excited with an ultra-short pulse, and consequently a single-cycle THz pulse is generated [27]. The generated signal was measured to have peak frequency of about 1 – 1.5 THz, and bandwidth of ~ 3 – 4THz [26,27]. Since the meta-atoms are designed to support localized surface plasmon resonances at the NIR regime, their nanoscale size is deep-subwavelength relative to the THz wavelength (i.e. ~1000 times smaller). Therefore, each excited nonlinear element can be treated as a dipole emitting a single-cycle THz pulse. Moreover, the capability to manipulate each meta-atom individually and locally, allows to engineer the spatial structure of the nonlinear response of the metasurface, and consequently the emitted waveform.

It was experimentally shown, that a periodic modulation of the orientation of the meta-atoms in the NLMS, results in a few-cycles THz pulse, with a varying carrier frequency according to the emission angle [26]. In this work, we show theoretically that this can be treated as a manifestation of direct space to time pulse-shaping (DST), that was previously demonstrated in the optical domain [28–32]. We show that this concept can be generalized to the generation of tailored THz pulse shapes based on the unique capabilities of engineered NLMS.

2. Mathematical description

We consider a NLMS with varying nonlinear response $s(x)$ along the x -axis. Under NIR excitation, at normal incidence to the metasurface, the generated THz amplitude profile $E(x, z = 0)$ is proportional to the nonlinear response structure:

$$E(x, z = 0) \propto s(x) \quad (1)$$

where z is the coordinate along the normal to the metasurface. The NLMS nonlinear response structure, $s(x)$, is decomposed to spatial Fourier components, i.e. to planar wave components with k_x momentum along the x -axis:

$$S(k_x) = \frac{1}{\sqrt{2\pi}} \int s(x) e^{-ik_x x} dx \quad (2)$$

whereas the inverse Fourier transform retrieves the spatial structure:

$$s(x) = \frac{1}{\sqrt{2\pi}} \int S(k_x) e^{ik_x x} dk_x \quad (3)$$

The temporal shape of the emitted pulse, $f(t)$ is decomposed to its temporal Fourier components, $F(\omega)$ so that:

$$F(\omega) = \frac{1}{\sqrt{2\pi}} \int f(t) e^{i\omega t} dt \quad (4)$$

and

$$f(t) = \frac{1}{\sqrt{2\pi}} \int F(\omega) e^{-i\omega t} d\omega \quad (5)$$

The spatiotemporal structure of the field on the metasurface is therefore:

$$E(x, t, z = 0) \propto s(x)f(t) = \frac{1}{2\pi} \int d\omega \int dk_x S(k_x) F(\omega) e^{i(k_x x - \omega t)} \quad (6)$$

During propagation of the emitted pulse along the z -axis, each momentum component accumulates phase $k_z(k_x)z = \sqrt{\left(\frac{\omega}{c}\right)^2 - k_x^2} z$, resulting in:

$$E(x, t, z) \propto \frac{1}{2\pi} \int d\omega \int dk_x S(k_x) F(\omega) e^{i(k_x x - \omega t)} e^{i\sqrt{\left(\frac{\omega}{c}\right)^2 - k_x^2} z} \quad (7)$$

The collection of light at specific angle at the far field, $\theta = \arctan\left(\frac{x}{z}\right)$, means that the collected field carries only a specific momentum component $k_x = \frac{\omega}{c} \sin\theta$. Mathematically, it is introduced to Eq. (7) as Dirac's delta function:

$$E(x, t, z) \propto \frac{1}{2\pi} \int d\omega \int dk_x S(k_x) F(\omega) e^{i(k_x x - \omega t)} e^{i\sqrt{\left(\frac{\omega}{c}\right)^2 - k_x^2} z} \delta\left(k_x - \frac{\omega}{c} \sin\theta\right) \quad (8)$$

Integrating over k_x gives the field at the collection site:

$$E(x = z \cdot \tan\theta, t, z) \propto \frac{1}{2\pi} \int d\omega S\left(\frac{\omega}{c} \sin\theta\right) F(\omega) e^{-i\omega\left(t - \frac{z}{c \cdot \cos\theta}\right)} \quad (9)$$

Which is simply a convolution between the kernel pulse form, i.e. the pulse shape of the single-cycle generated by the meta-atom, delayed by $t_0 = \frac{z}{c \cdot \cos\theta}$, and the metasurface structure

directly mapped to time according to $t = \sin\theta \frac{x}{c}$

$$E(x = z \cdot \tan\theta, t, z) = s\left(\frac{ct}{\sin\theta}\right) * f(t - t_0) \quad (10)$$

Qualitatively, all the meta-atoms are excited at the same time and generate synchronized pulses. When measured at an angle relative to the normal to the surface, the pulses are delayed with respect to each other, according to their origin on the metasurface. Therefore, the spatial distances over the metasurface are mapped into temporal delays, and each point on the metasurface is convoluted with the propagated kernel pulse, as also described in Fig. 1(a).

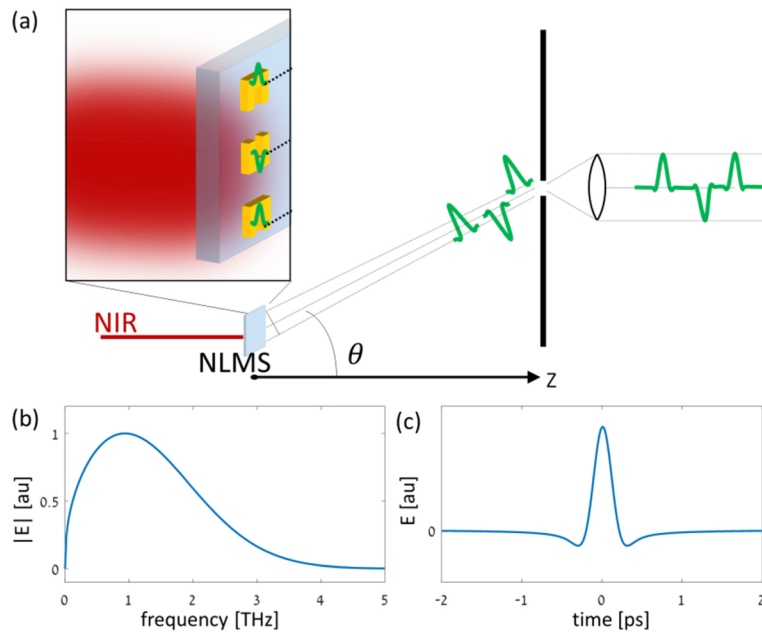


Fig. 1. (a) Working principle of THz-DST pulse shaping with NLMS. A near infrared ultrashort pulse (NIR) excites a NLMS consisted of nonlinear meta-atom. Consequently, each meta-atom emits a single-cycle THz pulse as a point source. When measured in the far-field at an angle θ (i.e., collected and collimated after a slit), a train of single-cycle pulses is formed. The train of pulses is formed according to the spatial distribution of the meta-atoms on the meta-surface, and the nonlinear response of each emitter. (b) THz emission spectrum from a NLMS based on SRRs as was experimentally measured before [26]. (c) Temporal form of THz pulse emitted from the NLMS.

The following numerical calculations are based on emission spectrum and kernel pulse shape that were experimentally measured before [26]. The spectral and temporal functions are shown in Figs. 1(b)-(c). The pulse duration is of $\Delta t \approx 1\text{ps}$, which defines the possible temporal resolution that can be achieved. We simulate the spatiotemporal structure of the pulse according to standard beam propagation technique that was extended to broadband pulses. This was done by numerical calculation of Eq. (7), which is based strictly on the Helmholtz equation.

3. Double pulse generation

To demonstrate this concept, we simulate a pulse emitted from a NLMS constructed of two regions of 0.2 mm and 0.4 mm, separated by 3.4 mm as depicted in Fig. 2(a). The calculated pulse shape for $\theta = 15^\circ$ and $z = 11\text{ cm}$ is shown in Fig. 2(b). It can be seen that the pulse shape

is consisted of two consecutive pulses with duration and amplitude proportional to the length of the region on the NLMS where they originate. The dashed line is the calculated convolution of the NLMS structure ($s(x)$) with the propagated kernel pulse ($f(t - t_0)$), according to Eq. (10). The concept of direct space to time mapping is even clearer when the carrier envelope of the pulse, i.e. the absolute value of the electric field, is compared with the NLMS structure. The carrier envelope shows the same general structural features as the spatial nonlinear response. Moreover, the carrier-envelopes of the convoluted pulse and simulated pulse show an exact match. The complete angle dependent emission pattern presented in Fig. 2(c) shows two branches, each associated with one of the regions on the NLMS. The time delay between the two generated pulses is changing with respect to the measurement angle, due to the angular dependence of the space-to-time mapping. This can be useful for single-shot pump-probe experiments, which usually require a delay line for adjusting the temporal delay between the pulses. Here, all the time differences can be realized at once. One must note however, that the duration of the actual pulses changes as well according to the DST mapping. Another potentially useful feature is that the structure of the pulses is reversed when measured at a negative angle. This occurs due to the anti-symmetric behavior of the DST mapping.

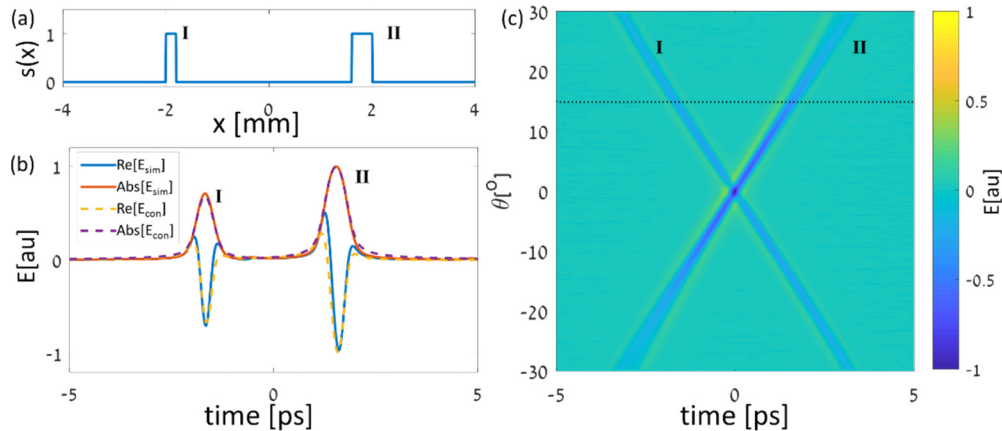


Fig. 2. (a) Structure of NLMS constructed of two separated regions of uniform arrays of SRRs, marked I and II. (b) Real part (Re) and absolute value (Abs) of calculated pulse shape for $\theta=15^\circ$ according to simulation (sim) and convolution (con) as described in Eq. (10). Pulses are associated with regions I and II (c) Angular dependent emission pattern as simulated by broadband beam propagation technique. Dashed line corresponds with (b).

4. Phase and amplitude modulation

One of the prominent advantages of metasurfaces in general, and NLMS for THz generation specifically, is the capability to tailor the optical response at each point on the surface. Recently it was shown that inversion of the SRR results with opposite phase of the emitted THz pulse (See Fig. 3(a)), which allows binary engineering of the wavefront by spatial arrangement of the SRRs orientation on the NLMS [26]. In addition to the discussed phase control, we suggest here additional degree of freedom for pulse shaping, given by varying the amplitude of the local emitted field. One method to control the amplitude of the emitted field is by clever detuning of the geometrical structure of the single meta-atom as was shown before for second harmonic generation [33,34]. Another way is to control the local concentration of the meta-atom, as depicted in Fig. 3(a). In the latter case, it is necessary to take into account the near-field effects [35], and additional collective effects, such as surface lattice resonances [36] that occur when the

meta-atoms have particular spacing. Such collective effects result in non-linear ratio between the concentration of meta-atoms and the effective local nonlinear response, and in addition the emission phase is modified. The spatial resolution of the phase and amplitude variance is determined by the size single unit cell of the metasurface, in the order of several hundreds of nanometers, which is deep-subwavelength relative to the emitted THz waves. Therefore the function $s(x)$ can be manifested on the metasurface continuously by local manipulation of the meta-atomic structure. The only constraint in this context is the maximal value of $s(x)$, which can be engineered to be the maximal available THz pulse amplitude emitted from a meta-atom.

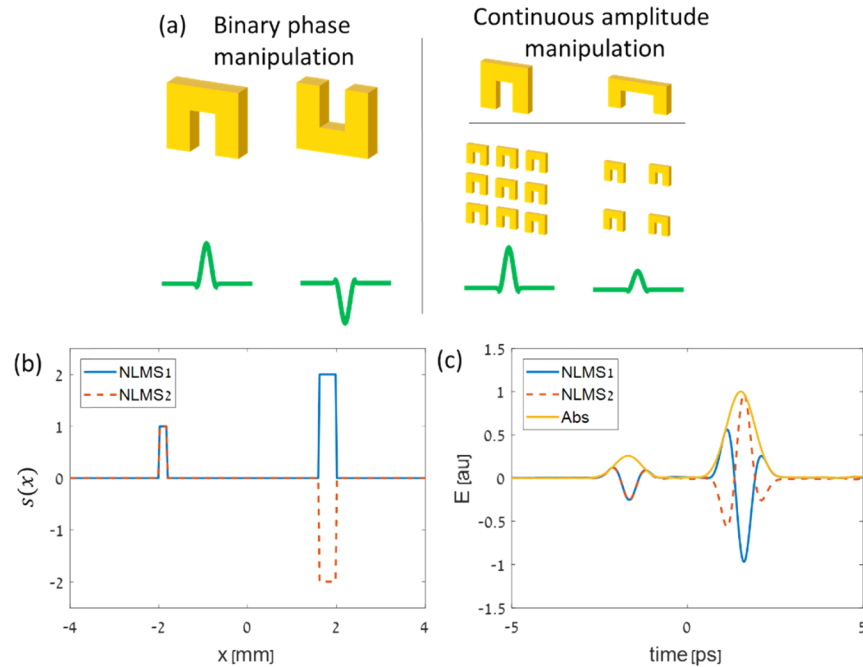


Fig. 3. (a) Illustration of methods to manipulate the local nonlinear response of the NLMS. The changes of the SRR array structure are shown at the top with the effect on the emitted pulse shown at the bottom. (b) Nonlinear response of studied two phase and amplitude modulated NLMS. (c) Simulated pulse shape emitted at 15° from NLMS structures presented in (b).

To demonstrate the effect of amplitude and phase modulation we analyze a modified version of the dual NLMS structure shown in the previous section. In the current case, the right-side region is characterized with double amplitude and either same (NLMS 1) or opposite (NLMS 2) phase of the local nonlinear response tensor relative to the left side region (Fig. 3(b)). The resulted pulse sequences are shown in Fig. 3(c). The amplitude difference between the pulses is evident as well as the effect of phase inversion. It can be seen that the absolute value of emission from NLMS 1 and NLMS 2 is equal while the phase of the right pulse is inverted between generation by NLMS 1 or NLMS 2.

5. Pulse reconstruction by deconvolution

The degrees of freedom for local THz emission with continuous amplitude and binary phase modulations, allow the generation of DST pulses by demand. According to Eq. (10), the spatial nonlinear response of the NLMS, $s(x)$, needed for the generation of an arbitrary pulse, can be

calculated by deconvolution of the desired pulse and the propagated kernel pulse:

$$s(x) = \mathcal{FT}^{-1} \left[\frac{\mathcal{FT} [E(\frac{x}{c} \sin \theta)]}{\mathcal{FT} [f(\frac{x}{c} \sin \theta - t_0)]} \right] \quad (11)$$

The deconvolution by division of the desired pulse and the kernel pulse Fourier components is problematic when calculated for frequencies which do not take part in the kernel spectrum due to the division in low values. Therefore, for the purpose of deconvolution, the spectra are truncated for frequencies higher than the maximal frequency, i.e. the highest frequency which has larger power than the noise of the system. This varies with the properties of the system, such as the type of NLMS, the pump pulse, and the detection scheme. Here the spectra were truncated above 3 THz.

To demonstrate reconstruction of a pulse, we present in Fig. 4(a) an arbitrary desired pulse shape (blue curve). The deconvolution of the pulse shape with the single-pulse kernel (purple curve), is presented by the yellow curve. This is used for the formation of the NLMS structure ($s(x)$), according to the DST mapping for $\theta=15^\circ$. The simulated pulse shape emitted from the calculated structure, $s(x)$, is shown in red curve. A very good agreement is obtained between the desired pulse and the emitted pulse. It is important to note that here the electric field itself is shaped, whereas most pulse shaping techniques including optical-domain DST usually treat only the carrier envelope. This method however, has fundamental limitations that originate from the limited bandwidth of the single-cycle kernel pulse. Temporal features that are shorter than the kernel pulse cannot be generated efficiently, due to the lack of the required high frequencies in the kernel pulse. On the other hand, long temporal features cannot be generated as-well due to the lack of low frequencies. These limitations are demonstrated in Fig. 4(b) in which a desired pulse is not reconstructed properly due to the short and long temporal features of the required pulse relative to the spectral content of the kernel pulse.

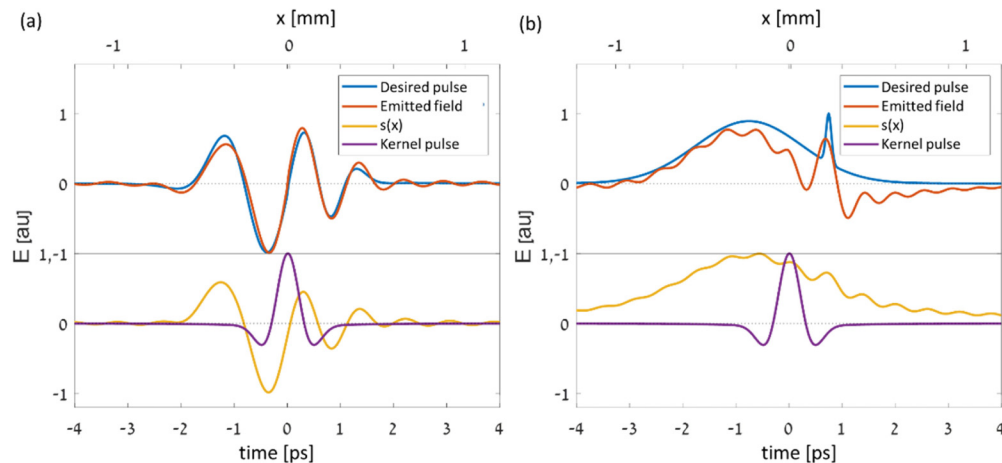


Fig. 4. (a) Reconstruction of desired pulse (blue) by deconvolution with the kernel pulse (purple) to calculate the required NLMS structure (yellow) for pulse emission at 30° . Red curve is the beam propagation simulated pulse. (b) Reconstruction of a desired pulse exceeding the bandwidth limitations.

6. Carrier envelope shaping

For some application the shape of the carrier envelope of short pulses can be instrumental. To achieve carrier envelope shaping using DST, a multiple cycles pulse with a certain carrier

frequency, ν , can be generated by a metasurface that has a sinusoidal nonlinear response with a periodicity Λ as follows:

$$\Lambda = \frac{c}{\nu \sin\theta} \quad (12)$$

This shows how the spatial periodicity is mapped to temporal frequency and vice versa. The resulting metasurface is conceptually identical to a nonlinear metasurface photonic crystal (NLMPs) for THz generation, as was described theoretically and experimentally before [26]. The direction of THz emission from NLMPs is usually calculated by momentum matching considerations, manifested in the nonlinear Raman-Nath diffraction condition. For normal incidence, this condition can be simplified to

$$\sin\theta = \pm \frac{\lambda}{\Lambda} \quad (13)$$

where, λ is the THz wavelength in the ambient medium. It can be seen how the latter expression is in fact identical to Eq. (12), which is derived according to the DST concept.

Next, the carrier envelope of the generated pulses can be shaped simply by multiplication of the periodic structure with the desired envelope.

Figure 5(a) demonstrates the design of an NLMS for generation of two consecutive pulses with different carrier frequencies, and arbitrary carrier-envelopes. The calculated emitted pulses at $\theta=30^\circ$ are composed of the carrier frequencies according to Eq. (12), with the corresponding carrier envelopes, as can be seen in Fig. 5(b). It is important to note that such arbitrary control of both carrier frequency and carrier envelope is very challenging to achieve by conventional pulse

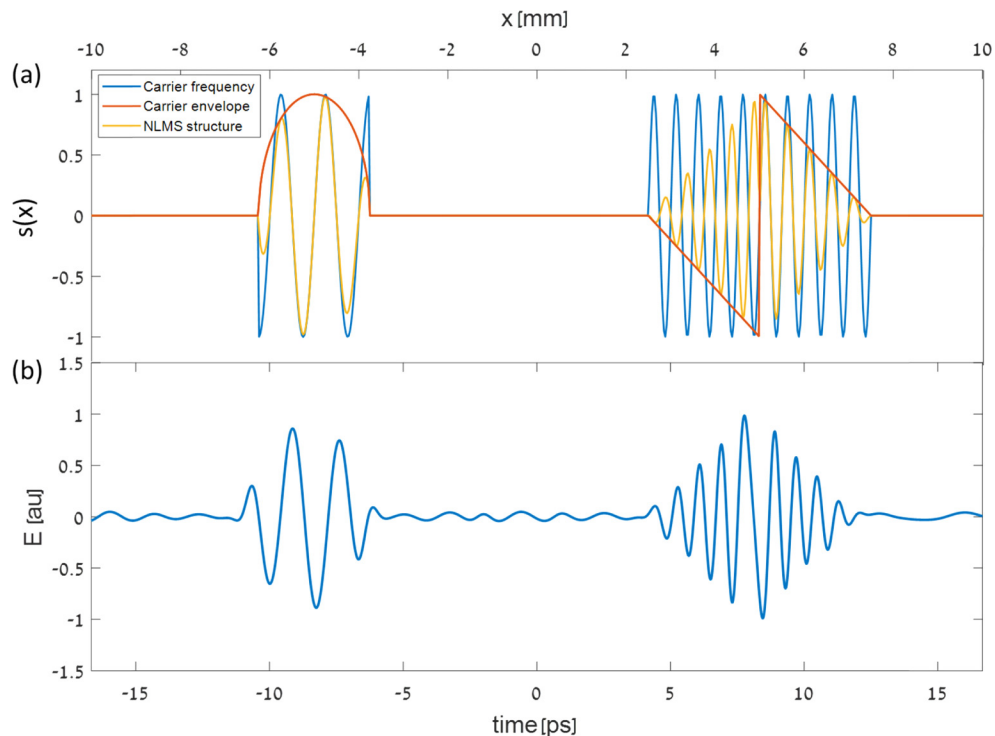


Fig. 5. (a) Design of a NLMS for generation of two consecutive pulses with different carrier frequency and envelope shape. (b) Emitted THz pulse at 30° from the NLMS described in (a).

shaping techniques. In addition, according to the same principle, the carrier frequency can be modified along the pulse (e.g. a chirped pulse) simply by using a NLMPC with a varying period.

7. All optical pulse shaping by pump manipulation

In the previous sections, we discussed the capability to shape the pulse according to the THz emission from the NLMS, which relies mostly on the location and emission characteristics of each of the meta-atoms on the NLMS. In this section we present the capability to use the NIR pump as a knob for controlling the emission from each meta-atom, consequently allowing all-optical control over the emitted THz pulse shape. One method to actively control the emission strength is by controlling the input polarization. Prior knowledge of the effective nonlinear tensor of the meta-atoms allows to calculate the pump polarization dependent emission. For example, it was shown that the SRRs that were used before, are excited by pump polarized parallel to the base of the SRR, and emit cross-polarized THz field. Assuming this is the most significant component of the effective nonlinear tensor, we can change the polarization angle ϕ of the pump beam in order to reduce the THz amplitude proportionally to the pump projection on the SRR base. This can be used for more versatile control of the emitted pulse by using various orientation of the meta-atom along the NLMS.

Figure 6(a) shows an NLMS built from two NLMS regions (similar to the NLMS in Fig. 2), each of them consisted of SRRs rotated at 90° relative to each other. For the calculations in Fig. 6(b) we take the assumption of quadratic interaction with dominant $\chi_{yxx}^{(2)}$ component, where x is the SRR base axis, according to the report by Luo et al [27]. As shown in Fig. 6(b), this allows to generate two consecutive pulses with actively controlled amplitude ratio. While this example

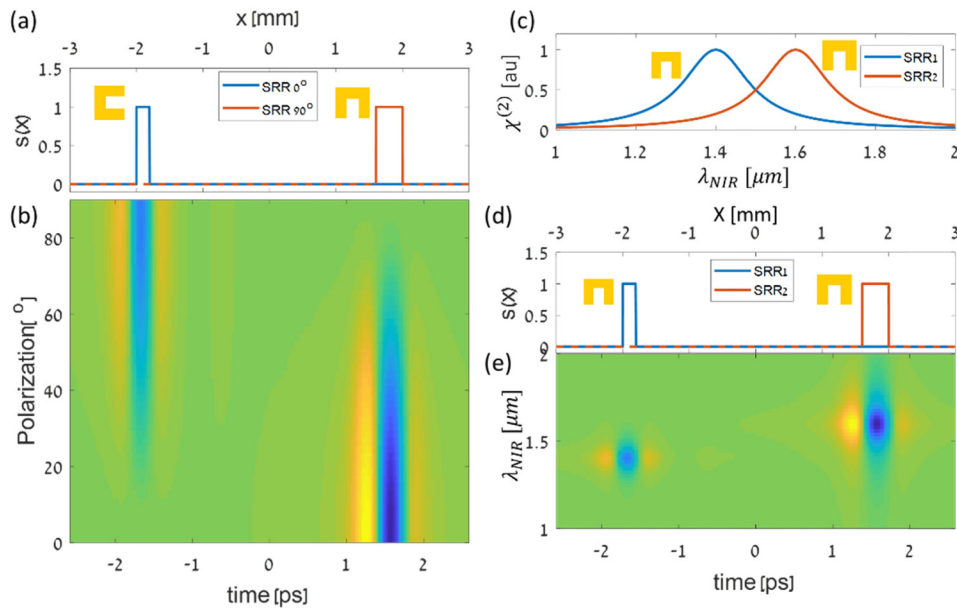


Fig. 6. (a) Structure of a NLMS consisted of two perpendicular oriented SRRs. (b) Emitted THz pulse from the NLMS described in (a), at 15° for various pump polarization. (c) Nonlinear coefficient dependency on NIR pump wavelength. Different resonant behavior is shown for two SRRs with different geometry. (d) NLMS structure consisted of two SRRs with different geometry and resonance frequency, as described in (c). (e) Emitted THz pulse from the NLMS described in (d) at 15° , for various pump wavelengths.

consists of separate regions with different types of meta-atom, in general interweaving different types of meta-atoms can be used to achieve more complex pulse structures. Furthermore, thanks to the ability to control the polarization of the emitted light (i.e., by the orientation of the SRRs), pulses with mixed polarization states can be generated as well. It is important to notice that this simplified description does not take into account additional nonlinear response tensor terms that might exist in a nonlinear meta-atom, and requires further investigation and optimization.

Another method to manipulate the strength of the interaction between the pump beam and the meta-atoms is by using their frequency response. Previous works have shown that the THz emission, e.g. from SRRs, strongly depends on the plasmonic resonances of the meta-atom. The localized surface plasmon resonance can be tuned by geometrical considerations. Therefore, using more than a single size of the meta-atoms along the NLMS, can result in active pulse shaping by changing the pump wavelength. For example, we assume two different SRRs building blocks, each with a different resonant response, as described in Fig. 6(c). The construction of a NLMS with two regions, each constructed of SRRs with different resonance frequency, as described in Fig. 6(d), results in pump wavelength-controlled pulse shapes. Specifically, the amplitude ratio between the two emitted pulses is modified by the pump wavelength, as shown in Fig. 6(e).

The demonstrations presented above for all-optical control of the emitted THz pulse shape show the principle in a highly simplistic way. The all-optical control knobs can be used to generate many more complex functionalities, e.g. optical control over the carrier frequency, optical manipulation of the length of the pulse, and multiplexing of various pulse shapes. The unique features of NLMS that allow the mentioned pulse shaping capabilities are accompanied, in principle, to the conventional pump controlled pulse shaping techniques that were presented before, e.g. spatial and temporal shaping of the pump [14].

8. Conclusion

We have shown that nonlinear metasurfaces provide a versatile platform for the generation of THz pulses with an engineered temporal shape. The treatment of each THz emitting meta-atom as a single-cycle source with tunable phase and amplitude, allows tailoring the temporal structure of the THz field emitted at a certain direction, by their arrangement along the metasurface, corresponding to DST concept. Calculations show that the emitted pulse shape takes the form of the convolution between the meta-atoms single-cycle pulse, and the metasurface structure directly mapped to time according to $t = \sin\theta \frac{x}{c}$. We show that this allows to use deconvolution in order to design structures that emit pulses with desired shape, within the constraints of bandwidth limitations. In addition, we provide several examples for exploiting the unique capabilities of structured nonlinear metasurfaces for various pulse shaping functionalities. We show that single, dual, or trains of few-cycle pulses with tailored envelopes and carrier frequencies can be generated. For generation of dual, or trains of pulses, emission to different angles shows a continuous delay between the pulses. This may be very interesting for various pump-probe, or coherent control applications. Moreover, pulses that are generated to positive and negative angles show an interesting time reversal relation. Finally, we also show that the pulses encoded on the NLMS can be different for each pump polarization state or excitation wavelength, allowing all-optical control over the emitted pulse shape, and advanced multiplexing.

The presented technique is based on one dimensional modulation, however, exploiting the two-dimensional nature of the NLMS suggests even more versatile control over the emission. For example, enhanced efficiency can be obtained at a focal point by circular arrangement of the meta-atoms [32], or flexible spatiotemporal wavepacket formation. The concept of a three-dimensional nonlinear metamaterial is even more intriguing and may expand the capability to control the generated THz wavepacket. Exploration of the THz generation mechanism in metasurfaces, along with extensive optimization can bring to significant enhancements to the

conversion efficiency and bandwidth control [37–39], which will improve the pulse shaping prospects.

Funding

H2020 European Research Council (ERC) (715362), Tel Aviv University (TAU) Center for Renewable Energy, Ministry of Science and Technology, Israel Scholarship for Ph.D. students in the applied sciences.

References

1. H. Y. Hwang, S. Fleischer, N. C. Brandt, B. G. Perkins, M. Liu, K. Fan, A. Sternbach, X. Zhang, R. D. Averitt, and K. A. Nelson, "A review of non-linear terahertz spectroscopy with ultrashort tabletop-laser pulses," *J. Mod. Opt.* **62**(18), 1447–1479 (2015).
2. I. A. Finneran, R. Welsch, M. A. Allodi, T. F. Miller, and G. A. Blake, "Coherent two-dimensional terahertz-terahertz-Raman spectroscopy," *Proc. Natl. Acad. Sci. U. S. A.* **113**(25), 6857–6861 (2016).
3. M. Woerner, W. Kuehn, P. Bowlan, K. Reimann, and T. Elsaesser, "Ultrafast two-dimensional terahertz spectroscopy of elementary excitations in solids," *New J. Phys.* **15**(2), 025039 (2013).
4. T. Kampfrath, A. Sell, G. Klatt, A. Pashkin, S. Mährlein, T. Dekorsy, M. Wolf, M. Fiebig, A. Leitenstorfer, and R. Huber, "Coherent terahertz control of antiferromagnetic spin waves," *Nat. Photonics* **5**(1), 31–34 (2011).
5. J. Lu, X. Li, H. Y. Hwang, B. K. Ofori-Okai, T. Kurihara, T. Suemoto, and K. A. Nelson, "Coherent Two-Dimensional Terahertz Magnetic Resonance Spectroscopy of Collective Spin Waves," *Phys. Rev. Lett.* **118**(20), 207204 (2017).
6. S. Fleischer, Y. Zhou, R. W. Field, and K. A. Nelson, "Molecular Orientation and Alignment by Intense Single-Cycle THz Pulses," *Phys. Rev. Lett.* **107**(16), 163603 (2011).
7. B. E. Cole, J. B. Williams, B. T. King, M. S. Sherwin, and C. R. Stanley, "Coherent manipulation of semiconductor quantum bits with terahertz radiation," *Nature* **410**(6824), 60–63 (2001).
8. S. Koenig, D. Lopez-Diaz, J. Antes, F. Boes, R. Henneberger, A. Leuther, A. Tessmann, R. Schmogrow, D. Hillerkuss, R. Palmer, T. Zwick, C. Koos, W. Freude, O. Ambacher, J. Leuthold, and I. Kallfass, "Wireless sub-THz communication system with high data rate," *Nat. Photonics* **7**(12), 977–981 (2013).
9. L. Möller, J. Federici, A. Sinyukov, C. Xie, H. C. Lim, and R. C. Giles, "Data encoding on terahertz signals for communication and sensing," *Opt. Lett.* **33**(4), 393 (2008).
10. A. M. Weiner, "Ultrafast optical pulse shaping: A tutorial review," *Opt. Commun.* **284**(15), 3669–3692 (2011).
11. A. M. Weiner, J. P. Heritage, and E. M. Kirschner, *High-Resolution Femtosecond Pulse Shaping* (1988), Vol. 5.
12. Y. Silberberg, "Quantum Coherent Control for Nonlinear Spectroscopy and Microscopy," *Annu. Rev. Phys. Chem.* **60**(1), 277–292 (2009).
13. M. Sato, T. Higuchi, N. Kanda, K. Konishi, K. Yoshioka, T. Suzuki, K. Misawa, and M. Kuwata-Gonokami, "Terahertz polarization pulse shaping with arbitrary field control," *Nat. Photonics* **7**(9), 724–731 (2013).
14. J. Ahn, A. Efimov, R. Averitt, and A. Taylor, "Terahertz waveform synthesis via optical rectification of shaped ultrafast laser pulses," *Opt. Express* **11**(20), 2486 (2003).
15. Y. Liu, S.-G. Park, and A. M. Weiner, "Terahertz waveform synthesis via optical pulse shaping," *IEEE J. Sel. Top. Quantum Electron.* **2**(3), 709–719 (1996).
16. Y.-S. Lee, N. Amer, and W. C. Hurlbut, "Terahertz pulse shaping via optical rectification in poled lithium niobate," *Appl. Phys. Lett.* **82**(2), 170–172 (2003).
17. L. Gingras and D. G. Cooke, "Direct temporal shaping of terahertz light pulses," *Optica* **4**(11), 1416 (2017).
18. L. Gingras, W. Cui, A. W. Schiff-Kearn, J.-M. Ménard, and D. G. Cooke, "Active phase control of terahertz pulses using a dynamic waveguide," *Opt. Express* **26**(11), 13876 (2018).
19. A. G. Stepanov, J. Hebling, and J. Kuhl, "Generation, tuning, and shaping of narrow-band, picosecond THz pulses by two-beam excitation," *Opt. Express* **12**(19), 4650 (2004).
20. J. Lu, H. Y. Hwang, X. Li, S.-H. Lee, O.-P. Kwon, and K. A. Nelson, "Tunable multi-cycle THz generation in organic crystal HMQ-TMS," *Opt. Express* **23**(17), 22723 (2015).
21. J. Yang, C. Gong, L. Sun, P. Chen, L. Lin, and W. Liu, "Tunable reflecting terahertz filter based on chirped metamaterial structure," *Sci. Rep.* **6**(1), 38732 (2016).
22. L. Ju, B. Geng, J. Horng, C. Girit, M. Martin, Z. Hao, H. A. Bechtel, X. Liang, A. Zettl, Y. R. Shen, and F. Wang, "Graphene plasmonics for tunable terahertz metamaterials," *Nat. Nanotechnol.* **6**(10), 630–634 (2011).
23. G. R. Keiser, N. Karl, P. Q. Liu, C. Tulloss, H.-T. Chen, A. J. Taylor, I. Brener, J. L. Reno, and D. M. Mittleman, "Nonlinear terahertz metamaterials with active electrical control," *Appl. Phys. Lett.* **111**(12), 121101 (2017).
24. L. Liu, X. Zhang, M. Kenney, X. Su, N. Xu, C. Ouyang, Y. Shi, J. Han, W. Zhang, and S. Zhang, "Broadband metasurfaces with simultaneous control of phase and amplitude," *Adv. Mater.* **26**(29), 5031–5036 (2014).
25. Y.-S. Lee and T. B. Norris, "Terahertz pulse shaping and optimal waveform generation in poled ferroelectric crystals," *J. Opt. Soc. Am. B* **19**(11), 2791 (2002).
26. S. Keren-Zur, M. Tal, S. Fleischer, D. M. Mittleman, and T. Ellenbogen, "Generation of spatiotemporally tailored terahertz wavepackets by nonlinear metasurfaces," *Nat. Commun.* **10**(1), 1778 (2019).

27. L. Luo, I. Chatzakis, J. Wang, F. B. P. Niesler, M. Wegener, T. Koschny, and C. M. Soukoulis, "Broadband terahertz generation from metamaterials," *Nat. Commun.* **5**(1), 3055 (2014).
28. D. E. Leaird and A. M. Weiner, "Femtosecond direct space-to-time pulse shaping," *IEEE J. Quantum Electron.* **37**(4), 494–504 (2001).
29. D. E. Leaird and A. M. Weiner, "Femtosecond direct space-to-time pulse shaping in an integrated-optic configuration," *Opt. Lett.* **29**(13), 1551 (2004).
30. J. D. McKinney, D. E. Leaird, and A. M. Weiner, "Millimeter-wave arbitrary waveform generation with a direct space-to-time pulse shaper," *Opt. Lett.* **27**(15), 1345 (2002).
31. A. Vega, D. E. Leaird, and A. M. Weiner, "High-speed direct space-to-time pulse shaping with 1 ns reconfiguration," *Opt. Lett.* **35**(10), 1554 (2010).
32. G. Mínguez-Vega, O. Mendoza-Yero, J. Lancis, R. Gisbert, and P. Andrés, *Diffractive Optics for Quasi-Direct Space-to-Time Pulse Shaping* (2008), Vol. 16.
33. K. O'Brien, H. Suchowski, J. Rho, A. Salandrino, B. Kante, X. Yin, and X. Zhang, "Predicting nonlinear properties of metamaterials from the linear response," *Nat. Mater.* **14**(4), 379–383 (2015).
34. S. Keren-Zur, O. Avayu, L. Michaeli, and T. Ellenbogen, "Nonlinear Beam Shaping with Plasmonic Metasurfaces," *ACS Photonics* **3**(1), 117–123 (2016).
35. S. Linden, F. B. P. Niesler, J. Förstner, Y. Grynko, T. Meier, and M. Wegener, "Collective Effects in Second-Harmonic Generation from Split-Ring-Resonator Arrays," *Phys. Rev. Lett.* **109**(1), 015502 (2012).
36. L. Michaeli, S. Keren-Zur, O. Avayu, H. Suchowski, and T. Ellenbogen, "Nonlinear Surface Lattice Resonance in Plasmonic Nanoparticle Arrays," *Phys. Rev. Lett.* **118**(24), 243904 (2017).
37. M. Fang, K. Niu, Z. Huang, W. E. I. Sha, X. Wu, T. Koschny, and C. M. Soukoulis, "Investigation of broadband terahertz generation from metasurface," *Opt. Express* **26**(11), 14241–14250 (2018).
38. M. Tymchenko, J. S. Gomez-Diaz, J. Lee, M. A. Belkin, and A. Alù, "Highly-efficient THz generation using nonlinear plasmonic metasurfaces," *J. Opt.* **19**(10), 104001 (2017).
39. M. Fang, N.-H. Shen, W. E. I. Sha, Z. Huang, T. Koschny, and C. M. Soukoulis, "Nonlinearity in the Dark: Broadband Terahertz Generation with Extremely High Efficiency," *Phys. Rev. Lett.* **122**(2), 027401 (2019).